Journal of Inorganic Biochemistry 162 (2016) 135–145

Contents lists available at ScienceDirect

Journal of Inorganic Biochemistry

journal homepage: www.elsevier.com/locate/jinorgbio

Ru(II)/clotrimazole/diphenylphosphine/bipyridine complexes: Interaction with DNA, BSA and biological potential against tumor cell lines and *Mycobacterium tuberculosis*

Legna Colina-Vegas [a,*], Jocely Lucena Dutra [a], Wilmer Villarreal [a], João Honorato de A. Neto [a], Marcia Regina Cominetti [b], Fernando Pavan [c], Maribel Navarro [d], Alzir A. Batista [a,*]

[a] Departamento de Química, Universidade Federal de São Carlos-SP, CEP 13565-905, Brazil
[b] Departamento de Gerontologia, Universidade Federal de São Carlos-SP, CEP 13565-905, Brazil
[c] Departamento de Ciências Biológicas, Faculdade de Ciências Farmacêuticas, UNESP, CEP 14800-900 Araraquara, SP, Brazil
[d] Directoria de Metrologia Aplicada a Ciências da Vida, Instituto Nacional de Metrologia, Qualidade e Tecnologia, INMETRO, RJ, Brazil

ARTICLE INFO

Article history:
Received 7 March 2016
Received in revised form 17 June 2016
Accepted 23 June 2016
Available online 25 June 2016

Keywords:
Ruthenium-bisdiphenylphosphine
Clotrimazole
Antitumor and anti-*Mycobacterium tuberculosis*

ABSTRACT

Three ruthenium complexes [RuCl(CTZ)(bipy)(P-P)]PF_6 [P-P = 1,2-bis(diphenylphosphino)ethane (dppe-**1**), 1,4-bis(diphenylphosphino)butane (dppb-**2**) and 1,1′-bis(diphenylphosphino)ferrocene (dppf-**3**), bipy = 2,2′-bipiridine and clotrimazole (CTZ) 1-[(2-chlorophenyl)diphenylmethyl]-1*H*-imidazole] were synthesized. These complexes were characterized by a combination of elemental analysis, molar conductivity, infrared and UV–vis spectroscopy, ^{1}H, $^{13}C\{^{1}H\}$ and $^{31}P\{^{1}H\}$ nuclear magnetic resonance techniques, cyclic voltammetry and mass spectroscopy. Bovine serum albumin binding constants, which were in the range of 1.30–36.00 × 10^{4} M^{-1}, and thermodynamic parameters suggest spontaneous interactions with this protein by electrostatic forces due to the positive charge of the complexes. DNA interactions studied by spectroscopic titration, viscosity measurements, gel electrophoresis, circular dichroism, ethidium bromide displacement and reactions with guanosine and guanosine monophosphate indicated the DNA binding affinity primarily through non-covalent interactions. All complexes **1**–**3** were tested against the human carcinoma cell lines MCF-7 (breast), A549 (lung) and DU-145 (prostate) presenting promising IC_{50} values, between 0.50 and 14.00 μM, in some cases lower than the IC_{50} for the reference drug (cisplatin). The antimicrobial activity assays of the complexes provided evidence that they are potential agents against mycobacterial infections, specifically against *Mycobacterium tuberculosis* H37Rv.

1. Introduction

Clotrimazole (CTZ), first synthesized by Karl Hienz Büchel in the late 1960s, was originally developed as an antifungal agent [1]. In addition there was promising research concerning the use of CTZ against other diseases, such as sickle cell anemia, malaria, beriberi, tineapedis, Chagas disease and cancer [2]. Thus, this organic compound has a broad spectrum of biological activity, high efficacy and minimal side effects. It was shown that clotrimazole is able to inhibit the proliferation of cancer cells *in vitro* and *in vivo*, as it inhibits enzyme activity involved in glycolysis stopping the cell cycle [3]. In 1993, the first metal complex containing clotrimazole was reported, $[RuCl_2(CTZ)_2]$, which showed high trypanocidal activity against Chagas disease, combined with low toxicity [4]. Furthermore, various authors have demonstrated that the CTZ coordination for Ru(II)-η^6-*p*-cymene, Au(I) and Cu(II) enhances its activity against the epimastigote form of *Trypanosoma cruzi*, indicating that all of them had their activity on parasite proliferation improved, when compared with the activity of the free CTZ [5–7]. CTZ metal complexes have shown potential applications in medicinal chemistry and synergistic effects were studied, thus, its metal complexes with ions such as Cu(II), Co(II), Ni(II), Zn(II) [8] and Pt(II) [9] had their cytotoxic activity improved (IC_{50} values) in cell growth inhibition of human carcinoma, when compared to the activity of the free ligand.

Biological activity of various ruthenium complexes stands out due to the ability of having action, *in vitro* and *in vivo*, against some tumor cell lines, as well as lower cytotoxicity, compared with platinum complexes. The structure of some of the most successful ruthenium complexes can be seen in Fig. 1, three Ru(III) anticancer agents: indazolium [*trans*-$RuCl_4$(1*H*-indazole)$_2$] (KP1019), sodium [*trans*-$RuCl_4$(1*H*-indazole)$_2$] (NKP-1339) and imidazolium [*trans*-$RuCl_4$(1*H*-imidazole)(DMSO-S)]

Abbreviations: CTZ, clotrimazole; bipy, 2,2′-bypiridine; BSA, bovine serum albumin; dppe, 1,2-bis(diphenylphosphino)ethane; dppb, 1,4-bis(diphenylphosphino)butane; dppf, 1,1′-bis(diphenylphosphino)ferrocene; MTB, *Mycobacterium tuberculosis*; DMSO, dimethyl sulfoxide; TBAP, tetrabutylammonium perchlorate; ATCC, America type culture collection; CT, calf thymus; EB, ethidium bromide; CD, circular dichroism; Ri, molar ratios; MTT, 3-(4,5-dimethylthiazol-2-yl-2,5-diphenyltetrazolium bromide; CFU, colony forming unit; MIC, minimum inhibitory concentration; K_{SV}, Stern–Volmer constant; K_q, biomolecular quenching rate constant; τ_o, average lifetime of the fluorophore.

* Corresponding authors.
E-mail addresses: esleg_24@hotmail.com (L. Colina-Vegas), daab@ufscar.br (A.A. Batista).

http://dx.doi.org/10.1016/j.jinorgbio.2016.06.023
0162-0134/

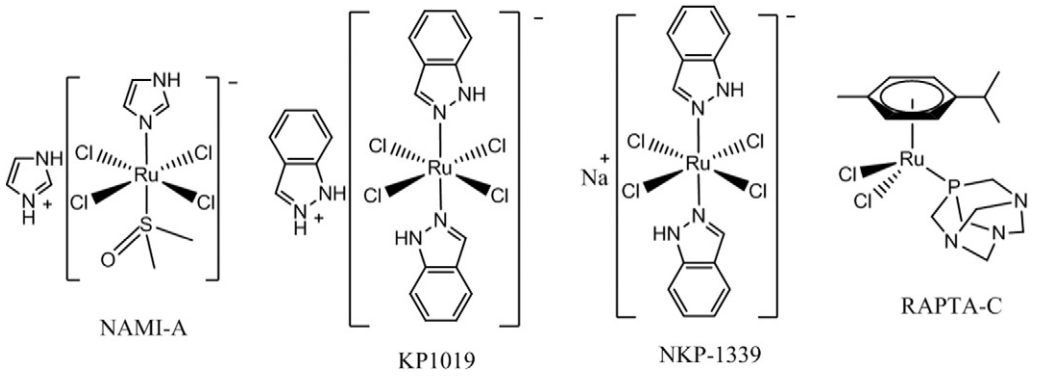

Fig. 1. Structure of the most promising ruthenium complexes in medicinal chemistry.

(NAMI-A) are currently undergoing clinical trials [10], and one Ru(II) complex: [Ru(*p*-cymene)Cl_2(1,3,5-Triaza-7-phosphaadamantane)] (RAPTA-C) also shows promising activities [11].

The potential use of ruthenium complexes for cancer treatment has motivated our research group to synthesize new Ru(II)-diphenylphosphine [12] and Ru(II)-triphenylphosphine [13] complexes and to test them against a range of tumor cells, yielding encouraging results. Thus, over the last seven years we have synthesized some ruthenium/phosphine/diimine complexes (Fig. 2), which showed promising activity against tumor cell lines, and also against *Mycobacterium tuberculosis* [14–18]. *M. tuberculosis* is the causative agent of tuberculosis, and in 2014 an estimated 9.6 million of new cases and 1.5 million died from this disease (1.1 million HIV-negative cases and 0.4 million HIV-positive cases) [19]. Treatment for *M. tuberculosis* (MTB) is expensive, long, it causes some side effects and encounters resistance. Therefore many researchers are looking for new alternative drugs to treat this illness. Thus, some ruthenium and gold complexes have been shown to be very propitious, with minimum inhibitory concentrations (MICs) comparable to, or even better than some reference drugs used to treat tuberculosis.

This paper describes the synthesis, spectroscopic and electrochemical characterization of three new complexes with the general formula [RuCl(CTZ)(bipy)(P-P)]PF_6, where P-P = 1,2-bis(diphenylphosphino)ethane (dppe, **1**), 1,4-bis(diphenylphosphino)butane (dppb, **2**) and 1,1′-bis(diphenylphosphino)ferrocene (dppf, **3**) and bipy = 2,2′-bipiridine. The diphenylphosphines were chosen as co-ligands in these complexes in order to stabilize the complexes due to their good π acceptor properties [20]. Here, we also present the preliminary *in vitro* tests of antimycobacterial and antitumor activities (A549, DU-145 and MCF-7) of the complexes. Finally, the interaction study of the synthesized ruthenium complexes with DNA by spectroscopic titration, viscosity measurements, gel electrophoresis, circular

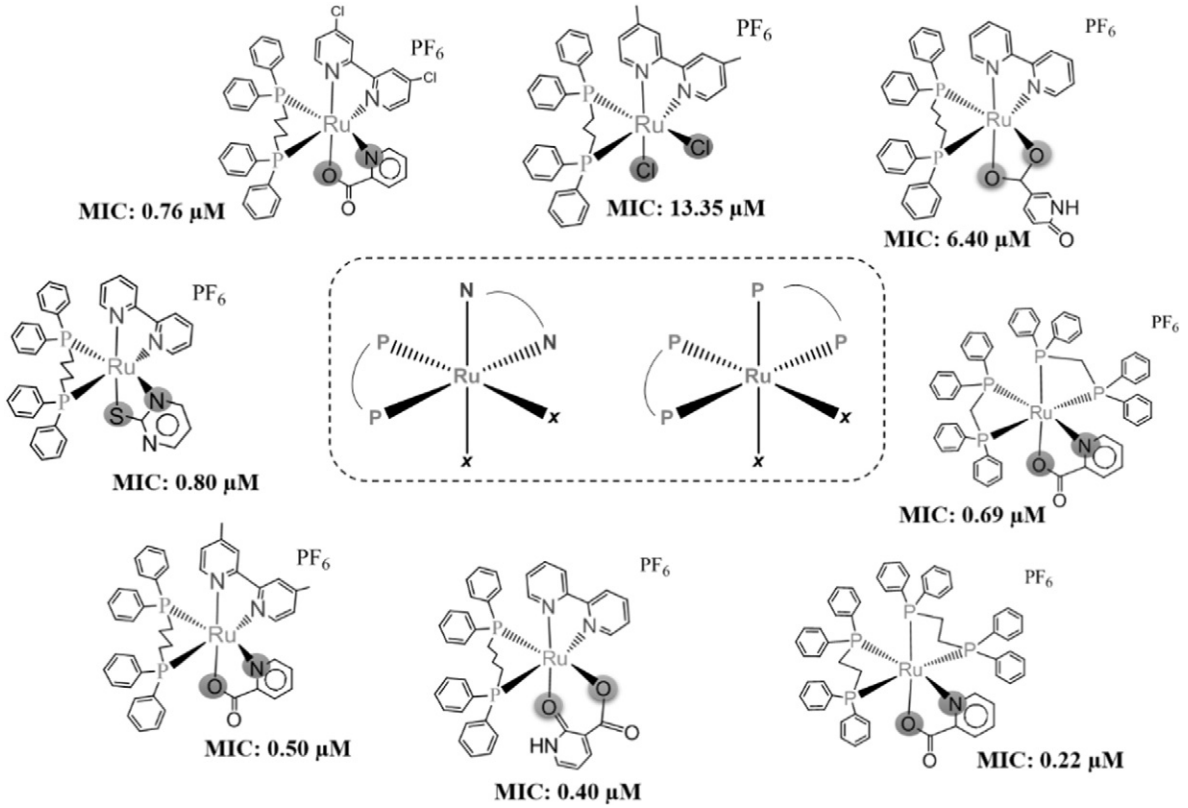

Fig. 2. Selected Ru(II)–bisdiphenylphosphine metal complexes with significant antimycobacterial properties prepared in our group [14–18].

dichroism, ethidium bromide (EB) displacement, guanosine and guanosine monophosphate, and with bovine serum albumin (BSA), by fluorescence quenching were carried out.

2. Experimental section

2.1. Materials and methods

All the syntheses of the complexes were performed under argon atmosphere. Solvents were purified by standard methods. All chemicals used were of reagent grade or comparable purity. The $RuCl_3 \cdot 3H_2O$ and the bis-(diphenylphosphine) ligands were purchased from Sigma-Aldrich. The precursors *cis*-[$RuCl_2$(P-P)(bipy)] were prepared according to the literature [21].

The electrochemical experiments were carried out using a BAS-100B/W MF-9063 Bioanalytical Systems Instrument under argon atmosphere at room temperature with tetrabutylammonium perchlorate (TBAP, FlukaPurum) as a supporting electrolyte. The electrochemical cell was equipped with platinum working and auxiliary electrodes and Ag/AgCl as the reference electrode in a Luggin capillary probe, a medium in which ferrocene is oxidized at 0.43 V (Fc^+/Fc). Voltammograms were performed at a scan rate of 0.100 V s^{-1}. The infrared spectra (IR) were recorded on a FTIR Bomem-Michelson 102 spectrometer in the range of 4000–200 cm^{-1} using CsI pellets. Conductivity data were obtained in acetone using a MeterLab CDM2300, measurements were made at room temperature using 1 mM solutions of the complexes. The ultraviolet–visible (UV–Vis) spectra of the complexes in CH_2Cl_2 were recorded on a Hewlett Packard diode array-8452A.

All the 1D and 2D NMR experiments (^{1}H, ^{13}C{^{1}H}, ^{31}P{^{1}H}, ^{1}H–^{1}H gCOSY, ^{1}H–^{13}C gHSQC, ^{1}H–^{13}C gHMBC) were recorded on a 9.4 T Bruker Avance III spectrometer with a 5 mm internal diameter indirect probe with ATMA™ (Automatic Tuning Matching), holding the temperature stable at 300 K. In general, 20 mg samples of CTZ and metal-CTZ complexes were dissolved in deuterated dimethylsulfoxide (DMSO-d_6, Cambridge Isotope Laboratories, Inc., USA). Mass spectra were obtained by direct infusion in a Waters Synapt Mass Spectrometer in positive ion mode, utilizing CH_3OCH_3 (LC/MS grade from Honeywell; B & J Brand) as the solvent.

2.2. Synthesis

General procedure (Scheme 1—reaction 6). A solution of *cis*-[$RuCl_2$(P-P)(bipy)] (0.100 mmol) in dichloromethane (25 mL) was stirred until complete dissolution was achieved, an excess of KPF_6 was added; after 1 h the CTZ (0.15 mmol) dissolved in dichloromethane was added. The resultant mixture was stirred and refluxed for 6 h under argon atmosphere. Afterwards, the final orange solutions were concentrated to *ca.* 2 mL and the solids were precipitated by adding n-hexane. The solids obtained were filtrated and washed with water (3 × 5 mL) to remove KPF_6 and KCl salts, n-hexane (3 × 5 mL) to remove CTZ in excess, and dried under vacuum.

[RuCl(CTZ)(dppe)(bipy)]PF_6 (**1**). Yield 92%; elemental analysis (%) Calc. for $C_{58}H_{49}Cl_2F_6N_4P_3Ru$ calc. (found) C 58.99 (58.98) H 4.18 (4.19) N 4.74 (4.69). Molecular weight (MW) 1180.92; IR: υ(C═C) 1485 cm^{-1}; υ(C═N) 1434 cm^{-1}; υ(P–C) 1000 cm^{-1}; υ(*P*–F) 842 cm^{-1}; δ(P–F) 557 cm^{-1}; υ(Ru–P) 503–526 cm^{-1}; υ(Ru–Cl) 316 cm^{-1}. UV–vis [(CH_2Cl_2) λ/nm (ε, M^{-1} L cm^{-1})]: 236 (42.090), 296 (17.175), 438 (2.098). ^{1}H NMR [400 MHz, DMSO-d_6, 298 K: δ ppm (*m*, I, attribution)]: 9.52, 8.54 and 8.25 (m, 4H, aromatic protons of bipy ligand), 7.70–6.40 (m, 41H, overlap of aromatic protons of dppe (20H), bipy (4H) and CTZ (17H) ligand), 3.08, 1.24 and 0.94 (m, 4H, CH_2 aliphatic of dppe ligand). ^{13}C{^{1}H} NMR [100.62 MHz, DMSO-d_6, 298 K: δ ppm (attribution)]: due to an overlap of the aromatic hydrogen, it was only possible to identify a set of signals at carbons, 158.10–122.91 (Cq and CH of dppe, bipy and CTZ ligands), 75.43 (C24-CTZ), 22.04 (CH_2-P of dppe ligand). ^{31}P{^{1}H} NMR [162 MHz, DMSO-d_6, 298 K: δ ppm (m, attribution)]: 65.70, 63.50 (d, P of dppe), −144.50 (h, PF_6). High resolution ESI(+)-MS (acetone): $[M + H]^+$ (1081.1761 *m/z*, 7.15%), $[M–PF_6]^+$ (1037.0835 *m/z*, 100.00%), $[M–CTZ–PF_6]^+$ (691.0082 *m/z*, 92.85%), [CTZ–Imidazol group]$^+$ (277.0487, 67.20%).

[RuCl(CTZ)(dppb)(bipy)]PF_6 (**2**). Yield 90%; elemental analysis (%) Calc. for $C_{60}H_{53}Cl_2F_6N_4P_3Ru \cdot H_2O$ calc. (found) C 58.73 (58.95) H 4.52

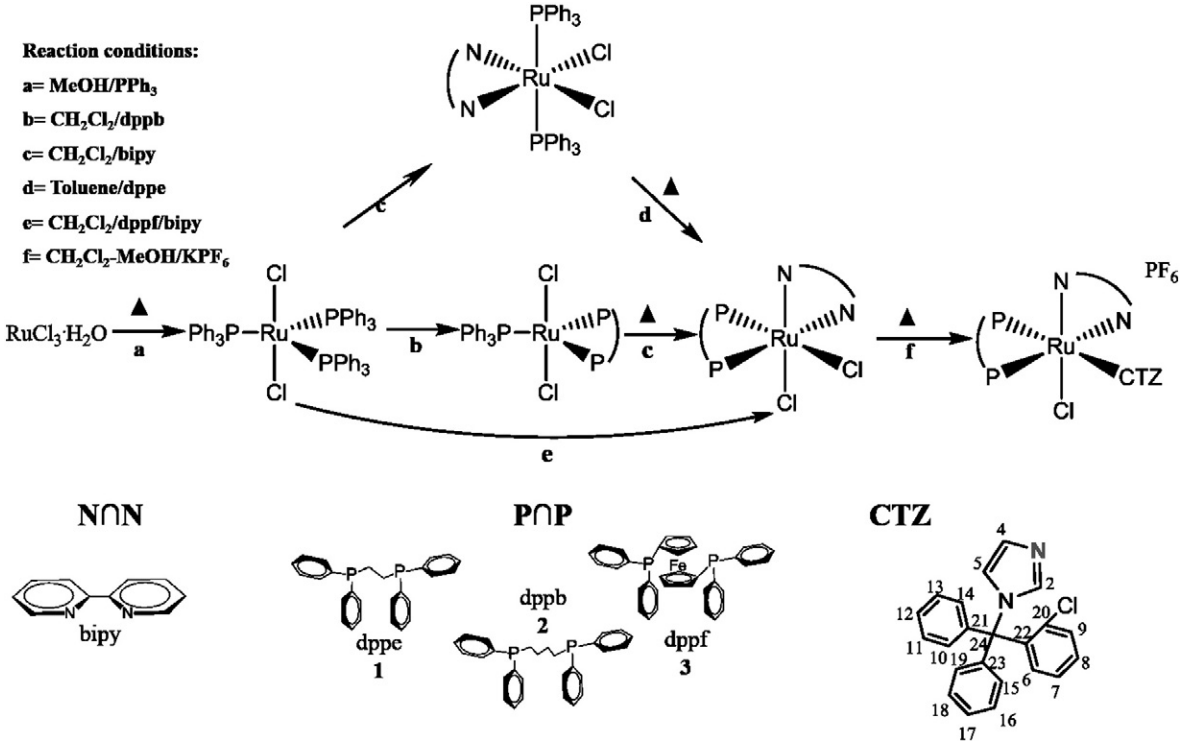

Scheme 1. Synthesis of the Ru(II)/clotrimazole/diphenylphosphine/bipyridine complexes.

(4.76) N 4.57 (4.67), MW: 1226.99; IR: υ(C═C) 1483 cm^{-1}; υ(C═N) 1434 cm^{-1}; υ(P–C) 1000 cm^{-1}; υ(P–F) 840 cm^{-1}; δ(P–F) 557 cm^{-1}; υ(Ru–P) 507–518 cm^{-1}; υ(Ru–Cl) 318 cm^{-1}. UV–vis [(CH_2Cl_2) λ/nm (ε, M^{-1} L cm^{-1})]: 236 (41.093), 298 (17.160), 458 (2.490). ^{1}H NMR [400 MHz, DMSO-d_6, 298 K: δ ppm (m, I, attribution)]: 8.73, 8.37, 7.90 (d, 6H, aromatic protons of bipy ligand),7.48–6.22 (m, 39H, overlap of aromatic protons of dppb (20H), bipy (2H) and CTZ (17H) ligand), 3.80, 3.20, 2.38 (m, 4H, aliphatics-CH_2-P of dppb ligand), 1.91, 1.45, 1.18 (m, 4H, aliphatics C-(CH_2)$_2$-C of dppb ligand). ^{13}C{^{1}H} NMR [100.62 MHz, DMSO-d_6, 298 K: δ ppm (attribution)]:due to an overlap of the aromatic hydrogen, it was only possible to identify a set of signals at carbons, 159.07–121.62 (Cq and CH of dppb, bipy and CTZ ligands), 74.95 (C24-CTZ), 27.88:25.83 (–CH_2-P of dppb ligand), 23.09:20.85 (C-(CH_2)$_2$-C of dppb ligand).^{31}P{^{1}H}NMR [162 MHz, DMSO-d_6, 298 K: δ ppm (m, attribution)]: 39.10, 37.40 (d, P of dppb), −144.50 (h, PF_6). High resolution ESI(+)-MS (acetone): $[M–PF_6]^+$ (1063.1721 *m/z*, 7.15%), $[M–CTZ–PF_6]^+$ (719.0262 *m/z*, 100%), [CTZ–Imidazol group]$^+$ (277.0487, 75.85%).

[RuCl(CTZ)(dppf)(bipy)]PF_6 (**3**). Yield 86%; elemental analysis (%) Calc. for $C_{66}H_{53}Cl_2F_6FeN_4P_3Ru$ calc. (found) C 59.30 (59.10) H 4.00 (4.39) N 4.19 (4.22), MW 1336.88; IR: υ(C═C) 1483 cm^{-1}; υ(C═N) 1433 cm^{-1}; υ(P–C) 1000 cm^{-1}; υ(P–F) 840 cm^{-1};δ(P–F) 547 cm^{-1}; υ(Ru–P) 511–520 cm^{-1}; υ(Ru–Cl) 349 cm^{-1}. UV–vis (CH_2Cl_2) λ/nm (ε, M^{-1} L cm^{-1}) 241 (46.275), 299 (20.148), 463 (3.773). ^{1}H NMR [400 MHz, DMSO-d_6, 298 K: δ ppm (*m*, I, attribution)]: 8.21, 6.52 (m, 45H, an overlap of aromatic protons of phenyl groups of dppf (20H), bipy (8H) and CTZ (17H) ligand), 4.99, 4.52, 3.58 (m, 8H, aromatic C–H ferrocene group of dppf). ^{13}C{^{1}H} NMR [100.62 MHz, DMSO-d_6, 298 K: δ ppm (attribution)]: due to an overlap of the aromatic hydrogen, it was only possible to identify a set of signals at carbons, 158.97–122.71 (Cq and CH of dppf, bipy and CTZ ligands), 75.37 (C24-CTZ), 73.92–72.97 (CH of dppf ligand).^{31}P{^{1}H} NMR [162 MHz, DMSO-d_6, 298 K: δ ppm (m, attribution)]: 38.40, 35.40 (d, P of dppf), −144.50 (h, PF_6). High resolution ESI(+)-MS (acetone): $[M–PF_6]^+$ (1191.0986 *m/z*, 7.15%), $[M–CTZ–PF_6]^+$ (846.9580 *m/z*, 83.33%), [CTZ–Imidazol group]$^+$ (277.0487, 75.85%).

2.3. Interaction studies

2.3.1. Spectroscopic measurements

All measurements with CT-DNA (calf thymus DNA from Sigma-Aldrich) were carried out in a Tris–HCl buffer (5 mM Tris–HCl and 50 mM NaCl, pH 7.4). The DNA concentration per nucleotide was determined by absorption spectrophotometric analysis using a molar absorption coefficient of 6.600 $mol^{-1}\cdot L\cdot cm^{-1}$ at 260 nm [22]. The spectroscopic titrations were carried out by adding increasing amounts of DNA to a solution of the complex, at a fixed concentration, in a quartz cell and recording the UV–vis spectrum after each addition. The intrinsic binding constant K_b was determined from the plot of [DNA] / ($\varepsilon_a - \varepsilon_f$) *vs* [DNA], where [DNA] is the concentration of DNA in base pairs, and the apparent absorption coefficients, ε_a, ε_f, and ε_b correspond to A_{obs} / [Ru] the extinction coefficient for the free ruthenium complex and ruthenium complex in the totally bound form, respectively. The data were fitted to Eq. (1), with a slope equal to 1 / ($\varepsilon_b - \varepsilon_f$) and the intercept equal to 1 / [$K_b(\varepsilon_b - \varepsilon_f)$] and K_b was obtained from the ratio of the slope to the intercept [23].

$$[DNA]/(\varepsilon_a-\varepsilon_f) = [DNA]/(\varepsilon_b-\varepsilon_f) + 1/[K_b(\varepsilon_b-\varepsilon_f)] \quad (1)$$

2.3.2. Viscosity experiments

Viscosity measurements were carried out using an Ostwald viscometer immersed in a water bath maintained at 25 °C. The DNA concentration in a Tris–HCl buffer was kept constant in all the samples, while the complex concentration was increased from 0 to 30 μM. The flow time was measured at least 5 times with a digital stopwatch and the mean value was calculated. Data are presented as $(\eta / \eta_0)^{1/3}$ *versus* the [complex]/[DNA] ratio, where η and η_0 are the specific viscosities of DNA in the presence and absence of the complex, respectively. The values of η and η_0 were calculated using the expression $(t - t_b) / t_b$, where t is the observed flow time and t_b is the flow time of the buffer alone.

2.3.3. Circular dichroism (CD) experiments

CD spectra were recorded on a spectropolarimeter JASCO J720 between 600 and 200 nm in a continuous scanning mode (200 nm/min). The final data are expressed in molar ellipticity (millidegrees). All of the CD spectra were generated and represented averages of three scans. Stock solutions (1.5 mM) of each complex were freshly prepared in DMSO prior to use. An appropriate volume of each solution was added to the samples of a freshly prepared solution of CT-DNA (100 μM) in a Tris–HCl buffer to achieve molar ratios ranging from 0.1 to 0.3 drug/DNA. The samples were incubated at 37 °C for 18 h.

2.3.4. Agarose gel electrophoresis studies

10 μL of pBR322 plasmid DNA in a Tris–HCl buffer were incubated at 37 °C for 20 h with molar ratios (Ri) of the Ru(II) compounds between 0.5 and 4.0. After incubation, 5 μL of each sample was separated by electrophoresis in a 1% agarose gel for 90 min at 100 V using a Tris borate–EDTA buffer (TBE) and stained with ethidium bromide (5 μL ethidium bromide per 50 mL agarose gel mixture). Samples of free DNA and DNA with DMSO were used as controls. The DNA bands were visualized as an image using a UV light transilluminator (ChemiDoc MP, Bio-Rad).

2.3.5. Ethidium bromide displacement

Assays were recorded on a spectrofluorimeter Spectra Max M3 in the 540–680 nm range with an excitation wavelength of 520 nm to solutions of CT-DNA (200 μM), EB (40 μM) and complex (100 μM), in Tris–HCl buffer at 25 °C.

2.3.6. Reaction with guanosine and 5′-guanosine monophosphate

The interaction between the Ru–CTZ complexes and DNA components was also studied and monitored by NMR spectroscopy making the ^{1}H and ^{31}P{^{1}H} NMR spectra at 25 °C in different time intervals. The study between complex **2** and guanosine monophosphate was carried out in DMSO:D_2O solutions. The interaction between complex **2** and the nucleotide guanosine was performed in DMSO.

2.3.7. Protein interaction

BSA (~2.5 μM) was prepared by dissolving the protein in Tris–HCl buffer and the complexes were dissolved in DMSO. The BSA concentration was determined by absorption spectrophotometric analysis using a molar absorption coefficient of 43.824 $mol^{-1}\cdot L\cdot cm^{-1}$ at 279 nm [24]. For fluorescence measurements, the BSA concentration in Tris–HCl buffer was kept constant in all the samples, while the complex concentration was increased from 0.78 to 100 μM, and quenching of the emission intensity of the BSA tryptophan residues at 340 nm (excitation wavelength 280 nm) was monitored at different temperatures (295 and 310 K). The experiments were carried out in triplicate and analyzed using the classical Stern–Volmer equation:

$$F_0/F = 1 + K_q\tau_o[Q] = 1 + K_{SV}[Q] \quad (2)$$

where F_0 and F are the fluorescence intensities in the absence and presence of the quencher, respectively, [Q] the quencher concentration, and *K*sv Stern–Volmer the quenching constant, which can be written as

$$K_q = K_{SV}/\tau_o \quad (3)$$

where K_q is the biomolecular quenching rate constant and τ_o is the average lifetime of the fluorophore in the absence of the quencher (~10^{-9} s) [25]. The binding constant (K_b) and number of complexes bound to BSA (n) were determined by plotting the double log graph

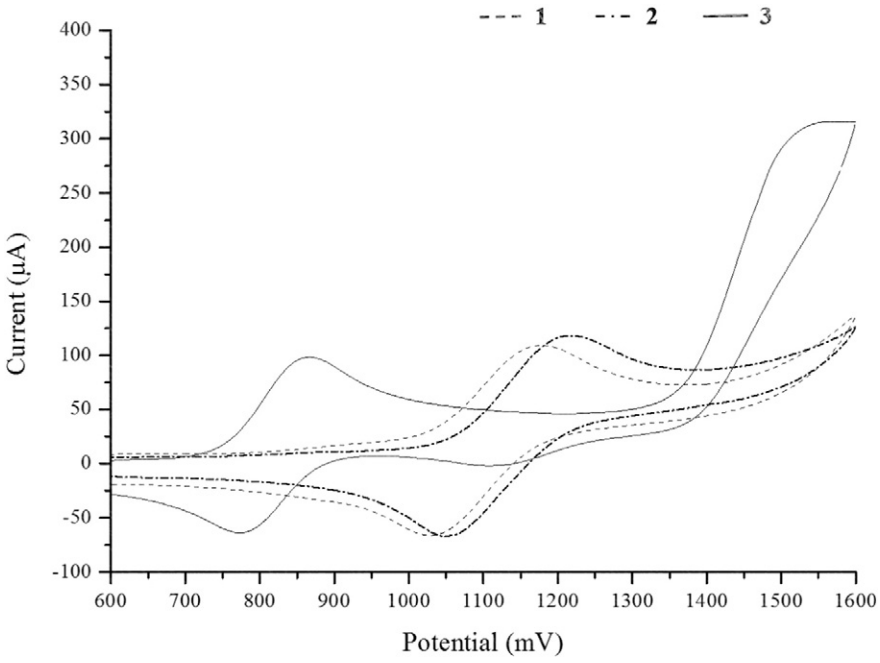

Fig. 3. Cyclic voltammogram for complexes [RuCl(CTZ)(bipy)(P-P)]PF_6 in CH_2Cl_2, (TBAP 0.1 M; Ag/AgCl; work electrode Pt; 100 $mV \cdot s^{-1}$).

of the fluorescence data using:

$$\log[(F_0 - F)/F] = \log K_b + n\log[Q]. \quad (4)$$

The thermodynamic parameter (ΔH) was calculated from equation:

$$\ln(K_2/K_1) = [(1/T_1) - (1/T_2)]\Delta H/R \quad (5)$$

where K_1 and K_2 are the binding constants at temperatures T_1 and T_2, respectively, and R is the gas constant. Furthermore, the change in free energy (ΔG) and entropy (ΔS) were calculated from the following equation:

$$\Delta G = -RT \ln K = \Delta H - T\Delta S. \quad (6)$$

2.3.8. Determination of octanol–water distribution coefficients (log D_{ow})

Water–octanol partition coefficients were determined using the shake flask method [26]. An UV–visible (UV–vis) calibration curve was prepared in the range 10–80 μM in n-octanol with 2% of dimethylsulfoxide for solubilization of the complexes. The determination was carried out at pH 7.4 in a mixture of equal volumes of water and n-octanol with 2% of dimethylsulfoxide and continuous shaking for 18 h at room temperature. The concentration of complex in n-octanol was measured spectrophotometrically in order to determine values of P = [compound] (in octanol) / [compouns] (in water).

2.4. Biological experiments

2.4.1. Cell viability assays

In vitro cytotoxicity assays on cultured human tumor cell lines still represent the standard method for initial screening of antitumor agents. Before performing the biological screening, the stability of the complexes was tested using the $^{31}P\{^1H\}$ NMR technique in DMSO solution containing 30% of Tris–HCl buffer. After 48 h, the spectra of the complexes were the same, when compared with those recorded using fresh solutions. Thus, as a first step to assess their pharmacological properties, the ruthenium complexes were assayed against human lung

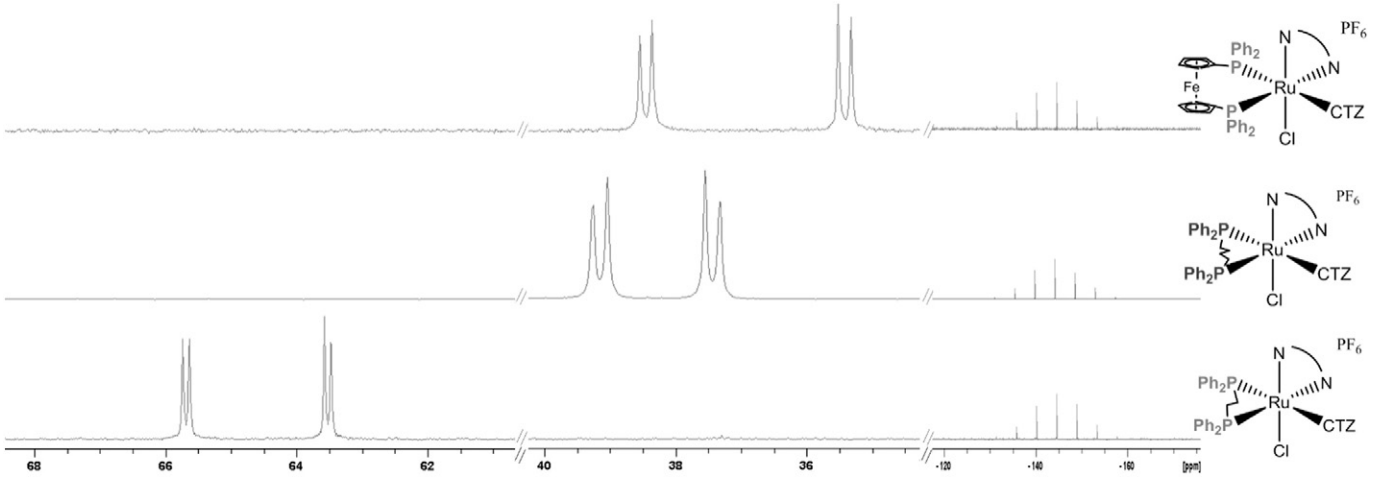

Fig. 4. $^{31}P\{^1H\}$ NMR spectra of complexes [RuCl(CTZ)(bipy)(P-P)]PF_6, in CH_2Cl_2/D_2O.

Table 1
Electrochemical, NMR $^{31}P\{^1H\}$ and molar conductivity data for complexes **1**–**3**.

	E_{pa} (mV)	E_{pc} (mV)	$E_{1/2}$	I_{pa}/I_{pc}	$^{31}P\{^1H\}$ (ppm)	$^{2}J_{(P-P)}$ (Hz)	Λ_M[a]
1	1164	1011	1087	1.14	63.5; 65.7	16.4	132.0
2	1135	1031	1083	1.22	37.4; 39.1	36.0	133.3
3	862/1570[b]	716/1375[b]	–	–	35.4; 38.4	28.5	123.2

[a] Λ_M: Ω^{-1} cm^2 mol^{-1}.
[b] FeII/FeIII potential values.

tumor line A549 (ATCC No. CCL-185), human prostate tumor line DU-145 (ATCC No. HTB-81), human breast tumor line MCF-7 (ATCC No. HTB-22), and the normal cell line L929 (ATCC No. CCL-1). The cells were routinely maintained with Dulbecco's Modified Eagle's medium (DMEM-for L929 and A549) or RPMI 1640 (for MCF-7 and DU-145) supplemented with 10% of fetal bovine serum (FBS), at 37 °C in a humidified 5% CO_2 atmosphere. For the cytotoxicity assay, 1.5×10^4 cells/well were seeded in 200 μL of complete medium in 96-well plates (Corning Costar). Each complex was dissolved in DMSO from 40 to 0.01 mM, 1 μL of each complex sample was added to 200 μL medium. Cells were exposed to the complex for a 48 h period. The conversion of MTT, 3-(4,5-dimethylthiazol-2-yl-2,5-diphenyltetrazolium bromide), to formazan by metabolically viable cells was monitored by an automated microplate reader at 540 nm.

2.4.2. Morphological observations

For the morphological study DU-145 prostate tumor cells were seeded at a density of 0.8×10^5 cells/well into 24-well plates. After allowing 24 h to adhere, images of cells treated, with or without complex **2**, were taken at 0, 2, 8, 24 and 48 h.

2.4.3. Antimycobacterial activity assay

The anti-*M. tuberculosis* activity of the ligands and of the ruthenium complexes was determined using the REMA (Resazurin Microtiter Assay) method [27]. Stock solutions of the compounds were prepared in DMSO and diluted in Middlebrook 7H9 broth (Difco, Detroit, MI, USA) supplemented with oleic acid, albumin, dextrose and catalase (OADC enrichment BBL/Becton-Dickinson, Sparks, MD, USA) so that final drug concentration ranges from 0.1 to 25 g·mL^{-1} could be obtained. The serial dilutions were performed in a Precision XS Microplate Sample Processor (Biotek™). The rifampicin was dissolved in distilled water, and used as a standard drug. A suspension of the MTB $H_{37}Rv$ ATCC 27294 was cultured in Middlebrook 7H9 broth supplemented with OADC and 0.05% Tween 80. The culture was frozen at −80 °C in aliquots. After two days the colony forming unit (CFU)/mL of an aliquot was carried out. The concentration was adjusted to 5.10^5 CFU/mL and 100 μL of the inoculum was added to each well of a 96-well microtiter plate together with 100 μL of the compound. Samples were set up in triplicate. The plate was incubated for 7 days at 37 °C. After 24 h, 30 μL of 0.01% resazurin (solubilized in water) was added. The fluorescence of the wells was read after 24 h using a TECAN Spectrafluor. The MIC was defined as the lowest concentration resulting in 90% inhibition of growth of MTB.

3. Results and discussion

3.1. Spectroscopic and analytical characterization

The reduction of ruthenium(III) chloride with excess of triphenylphosphine conducted in refluxing methanol, afforded the brown crystalline solid of neutral complex $[Ru^{II}Cl_2(PPh_3)_3]$, the triphenylphosphine serves as the reducing agent yielding triphenylphosphine oxide. As presented in Scheme 1, $[Ru^{II}Cl_2(PPh_3)_3]$ reacts with bidentate phosphine and bypiridine ligand in a sequence of substitution reactions to give the precursor *cis*-$[Ru^{II}Cl_2(P–P)(N–N)]$ that upon stirring and reflux, in dichloromethane solution, and the presence of CTZ result in the new cationic compounds **1**–**3**.

All three complexes were prepared in good yields (>85%), their general structures are proposed based on spectroscopical data, as well as elemental analyses, which were in good agreement with proposed formulations, molar conductivity measurements, and ^1H, $^{13}C\{^1H\}$ and $^{31}P\{^1H\}$ NMR spectra. Molar conductivities of **1**, **2** and **3** in acetone, were in the range of 1:1 electrolytes [28]. The electronic spectra for the complexes showed two bands in the UV region (240–300 nm) presents in the free ligands and assigned to π → π* transitions from the aromatic rings are also present in the spectra of the complexes, probably involving the phosphine, bipyridine and clotrimazole ligands [29,30], and one band in the visible region (~450 nm), which can be assigned as metal to ligand charge transfer transitions from Ru(dπ) to the ligand (π*), similar assignments have been proposed for other Ru(II) complexes [31,32] and previous work by this group [33]. The solid state

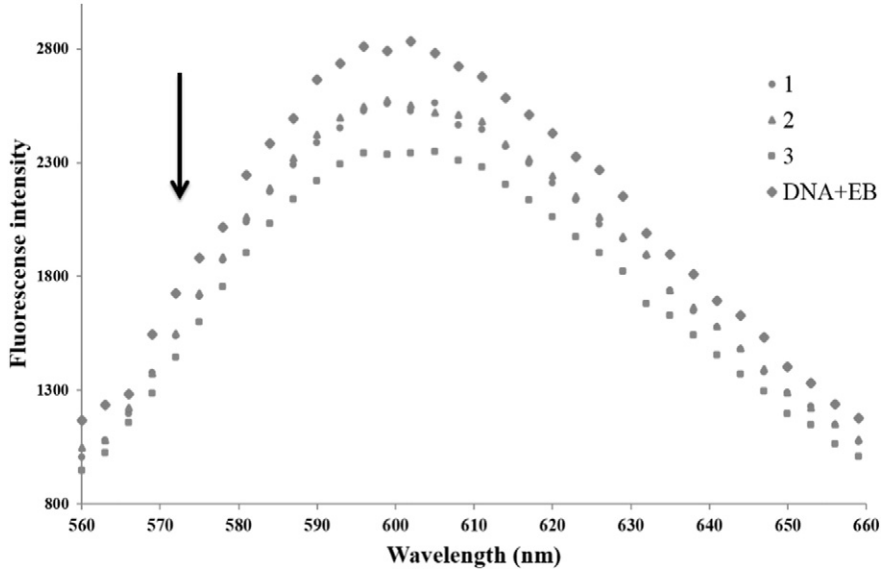

Fig. 5. Fluorescence spectra obtained from EB displacement assays. [CT-DNA] = 200 μM, [EB] = 40 μM and [Complex] = 100 μM, in Tris–HCl buffer at 25 °C.

FT-IR spectra of the complexes presented the characteristic band of Ru–P (502–521 cm^{-1}), PF_6^- (841 and 557 cm^{-1}), Ru–N (425–430 cm^{-1}), Ru–Cl (316–349 cm^{-1}) and the imidazole ring (CH stretch) in the range of 3057–3064 cm^{-1}.

The electrochemical behavior of the redox-active compounds were studied at room temperature using the cyclic voltammetry technique, at a platinum disk electrode, in dichloromethane with TBAP as a supporting electrolyte. The obtained voltammograms of the complexes are shown in Fig. 3. Complexes **1** and **2** showed a similar electrochemical behavior, a quasi-reversible one-electron Ru(III)/Ru(II) redox process, with a potential at about 1000 mV. For complex **3**, this process is around ~800 mV and other redox process ~1570 mV were also found, characteristics of the Fe(III)/Fe(II) couple from the ferrocene molecule in the dppf ligand. In order to confirm this, an electrolysis at 1570 mV was carried out and the product was reacted with NH_4SCN. The red solution obtained is a characteristic of the formation of $[Fe(SCN)_6]^{3-}$ species. As expected, the $E_{1/2}$ values found for the new complexes were considerably more anodic than those observed for the respective precursors, between 177 and 480 mV, indicating a more stabilized Ru(II) center in the new derivatives than in their precursors. This stabilization is suggested to be due to the substitution of chlorido (σ and π-donor) by an imidazole ring (σ-donor and π-acceptor). The proposed composition for the complexes were also confirmed by mass spectrometry analyses. The ESI(+)-MS spectra for complex **1**–**3** showed a signal corresponding to a protonated species $[M + H]^+$ (only for the complex **1**) and its fragmentations generating the product ion corresponding to the loss of hexafluorophosphate ion $[M–PF_6]^+$, followed by the loss of the clotrimazole ligand, forming the $[M–PF_6–CTZ]^+$ and a peak corresponding to the free ligand [CTZ–Imidazole group]$^+$.

The $^{31}P\{^1H\}$ NMR spectra of all complexes in CH_2Cl_2/D_2O (Fig. 4) present a typical AX spin system indicating the magnetic non-equivalence of the two phosphorus atoms, corresponding to the P *trans* N (bipy) and P *trans* N (CTZ). The chemical shifts and coupling constants ($^2J_{P\text{-}P}$) are shown in Table 1. In the precursors, *cis*-[Ru(bipy)(P-P)Cl_2], the high-field doublet corresponds to the P *trans* Cl, as previously described [34], the shift to higher energy is indicative of the coordination of the metal ions to the N3, from the CTZ ligand. The ^1H NMR spectra for all complexes showed signals for CTZ, bipyridine and the phosphine phenyl groups as a series of overlapped multiplets between the 9.20–6.20 ppm region, corresponding to 45 hydrogen atoms. Furthermore, additional multiplets for complexes **1** and **2** are observed corresponding to CH_2 groups of dppe (3.08, 1.24, 0.94 ppm) and dppb (3.80, 3.20, 2.38, 1.91, 1.45, 1.18 ppm), and for **3** attributed to ferrocene of dppf ligand (4.99, 4.52 and 3.58 ppm).

3.2. Biological targets: DNA and BSA binding studies

3.2.1. DNA binding studies

To explore the possibility of DNA as a potential target for the complexes, spectroscopic studies were carried out. UV–visible absorption spectroscopy is a versatile and normally engaged method to determine the binding characteristics of metal complexes with DNA. The intense absorption spectral band around 300 nm, observed for all complexes, were used to evaluate their possible interaction with CT-DNA, in Tris–HCl buffer at pH 7.4. The experiments were carried out keeping the concentration of the Ru(II) complexes constant, and varying the concentration of the CT-DNA. When adding the solution of CT-DNA to each complex **1**–**3**, a strong decrease in absorption intensity (hypochromism, ~36%) was observed. In order to compare the binding strength of the three complexes quantitatively, the intrinsic binding constant K_b was calculated using the neighbor exclusion equation (Eq. (1)). The K_b values are in the trend **3** > **1** ≈ **2** > CTZ. The K_b value for **3** (1.65×10^4 M^{-1}) is two-fold higher than for **1** and **2** (**1**: 0.90; **2**: 0.84×10^4 M^{-1}) and ten-fold higher than for the CTZ (0.16×10^4 M^{-1}), indicating higher binding affinities of **3** to CT-DNA, when compared with the other species. From the results obtained, it has been found that all Ru(II) complexes show a good binding affinity to DNA and the values lie within the interval for which a compound is considered to be interacting with DNA [35].

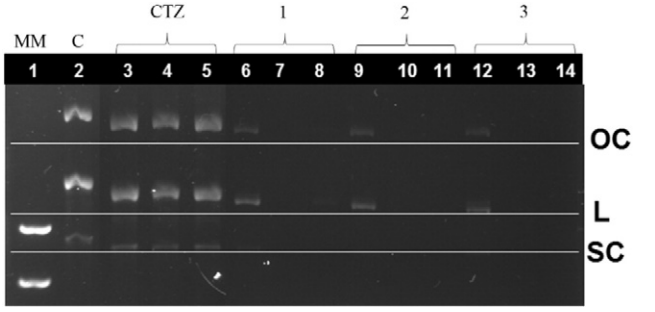

Fig. 6. Electrophoresis of plasmid pBR322 DNA incubated in 5 mM Tris–HCl buffer for 18 h at 37 °C treated with 0.5, 2.0 and 4.0 eq. of CTZ and complexes **1**, **2** and **3**. MM: molecular marker, C: control, pBR322 with DMSO.

Viscosity measurements are successfully used to determine if there are intercalation or non-intercalation binding modes of the complexes to DNA [36]. It is well known that classical intercalators, such as ethidium bromide, lead to an increase in the viscosity of CT-DNA, when in the presence of complexes, because separation of the base pairs occurs to accommodate the intercalator [37]. A covalent DNA-binding mode may cause its fragmentation, thus decreasing the DNA viscosity [38]. Thus, in this study it can be observed that the viscosity of the solution of CT-DNA did not change significantly when the concentration of the complexes **1**–**3** was increased, indicating that ruthenium complexes bind with DNA in a non-intercalative manner.

The CD spectral technique is very sensitive for diagnosing changes in the secondary structure of DNA, resulting from drug–DNA interactions. A typical CD spectrum of calf thymus CT-DNA shows a maximum at 275 nm, due to the base stacking and a minimum at 248 nm attributed to the right-handed helicity, characteristic of the B conformation. To determine if the Ru(II)–CTZ complexes cause changes in the helical structure of DNA, CD spectra of CT-DNA with increasing concentrations of compounds **1**–**3** and free CTZ were acquired, up to molar ratio drug/DNA (Ri): 0.3, and a significant change was not observed in the CD magnitude (see Fig. S7 in supplementary information).

Ethidium bromide (3,8-diamino-5-ethyl-6-phenyl phenanthridium bromide, EB) is a known DNA intercalator agent, widely used as a sensitive fluorescent probe for DNA due to its high fluorescence when bound to the nucleic acid. The free EB molecule shows reduced emission intensity as a consequence of the solvent quenching or of a photoelectron transfer mechanism [39], when bound to DNA, EB shows a remarkable enhancement in fluorescence, due to a steric protection that the nucleobases provide to the dye molecule [40]. The presence of another species with affinity toward DNA may result in a decrease in the emission intensity of the EB-DNA adduct, caused by either a competition for binding sites, a change in DNA conformation or through a

Table 2
Stern–Volmer quenching constant (K_{SV}, M^{-1}), biomolecular quenching rate constant (K_q, M^{-1} s^{-1}), binding constant (K_b, M^{-1}), the number of binding sites (n), ΔG° (KJ·mol^{-1}), ΔH° (KJ·mol^{-1}) and ΔS° (J·mol^{-1} K) values for the complex–BSA system at different temperatures.

		Ksv ($\times 10^4$)	K_q ($\times 10^{13}$)	K_b ($\times 10^4$)	n	ΔG	ΔH	ΔS
CTZ	295	0.22	1.39	0.06	1.20	−1.22	60.47	246.50
	310	0.22	1.39	0.05	1.77	−1.59		
1	295	1.48	9.18	1.36	0.85	−2.34	4.31	93.84
	310	1.52	9.43	1.43	1.03	−2.48		
2	295	1.77	10.91	1.49	0.75	−2.34	2.86	89.15
	310	1.90	11.77	1.49	0.63	−2.48		
3	295	3.74	23.19	3.30	0.87	−0.49	3.82	29.65
	310	3.93	27.37	3.36	0.90	−0.54		

Table 3
Biological activity of the ruthenium compounds against four tumor cell lines for 48 h incubation and distribution coefficient (log D) at pH 7.4

	IC_{50} (μM)				IS^1	IS^2	IS^3	log D
	A549	DU-145	MCF-7	L929				
CTZ	14.47 ± 0.95	15.82 ± 0.23	16.80 ± 2.52	9.74 ± 2.05	0.67	0.61	0.58	–
1	2.11 ± 0.15	3.64 ± 0.50	3.83 ± 0.12	2.61 ± 0.13	1.23	0.71	0.68	0.60 ± 0.06
2	0.47 ± 0.05	3.32 ± 0.45	1.68 ± 0.32	0.48 ± 0.05	1.02	0.14	0.28	0.48 ± 0.02
3	4.79 ± 0.40	7.40 ± 0.35	13.28 ± 1.00	5.89 ± 0.80	1.22	0.80	0.44	0.84 ± 0.10
Cisplatin[a]	14.42 ± 1.45	2.33 ± 0.40	13.98 ± 2.02	16.53 ± 2.38	1.14	7.09	1.18	–

[a] Reference drug. $IS^1 = IC_{50}L929/IC_{50}A549$; $IS^2 = IC_{50}L929/IC_{50}DU\text{-}145$, $IS^3 = IC_{50}L929/IC_{50}MCF\text{-}7$.

photoelectron transfer mechanism. EB displacement assays were performed to extract more information about the binding DNA and Ru(II)–CTZ complexes by monitoring the emission intensity of DNA-bound EB fluorescence. In Fig. 5, it can be observed that after adding the complexes (100 μM) to CT-DNA solution (200 μM) pretreated with EB, (40 μM) ([DNA]/[EB]: 5) in 5 mM of Tris–HCl, the emission intensity of DNA-bound EB decreases 9.90% (for **1**, **2**) and 17.30% (for **3**), which is consistent with the order of the above K_b values obtained by UV–Vis absorption spectral titration. This result indicates that **3** at higher concentrations would compete with DNA-bound EB more efficiently than **1** and **2**, and indicate that the complexes can partially displace the DNA-bound EB suggesting low to moderate competition with EB, this DNA binding behavior was observed previously for non-intercalative complexes containing CTZ like as Cu(II), Co(II), Ni(II), Zn(II) [8] and also complexes containing antimicrobial drugs ofloxacin (ofloH) and norfloxacin (nfH) with general formula: $[Cu(nfH)(phen)Cl]Cl$, $[Cu(nfH)_2]Cl_2$ and $[Cu(ofloH)_2][(CuCl_2)_2]$ [41].

The interaction of complexes **1**–**3** with pBR322 DNA was studied by agarose gel electrophoresis (Fig. 6) by incubating the Ru(II) complexes or free clotrimazole, with pBR322 DNA (40 μM) in Tris–HCl buffer at pH 7.4 for 18 h, at 37 °C, with Ri 0.5, 2.0 and 4.0. The control experiment in lane 2 shows the corresponding open circular, linear and super coiled form for untreated plasmid DNA. Lines 3-5 correspond to the plasmid incubated with clotrimazole, while lines 4–14 correspond to the plasmid incubated with different concentrations of complexes **1**, **2** and **3**. The CTZ ligand does not induce a noticeable alteration in the mobility of the plasmid, however it is clear that the increase in the concentration of each Ru(II)–CTZ complex caused remarkable changes in the mobility of the plasmid. Only two bands are evident for all complexes at R_i 0.5, representing both the linear and open circular forms. At R_i 2.0 and R_i 4.0, no bands (either relaxed or linear band) are visible for the DNA. The first possible explanation for this observation is that EB was completely expelled out of the plasmid due to DNA binding of the complex at higher concentrations, leading to quenching of the EB emission. Another alternative for this observed effect could be due to changes in the DNA structures, suggesting a strong interaction of the complexes with the plasmid, inhibiting the EB binding. In all likelihood, a combination of both effects probably occur: EB expels and changes in the DNA structure. Similar behavior was observed previously for the $[Ru(Hdpa)_2(diimine)]ClO_4$ [42] and $[Ru(bpy)(L)]PF_6$ complexes [43].

In conclusion, from all the data obtained it can be suggested that the Ru(II)–CTZ compounds present DNA binding affinity, primarily through weak interactions, such as hydrogen bonding by major or minor groove and/or electrostatic interactions involving the negatively charged phosphate groups of DNA, considering the positive charge of the complexes. Thus, in order to verify these observations, the reaction between

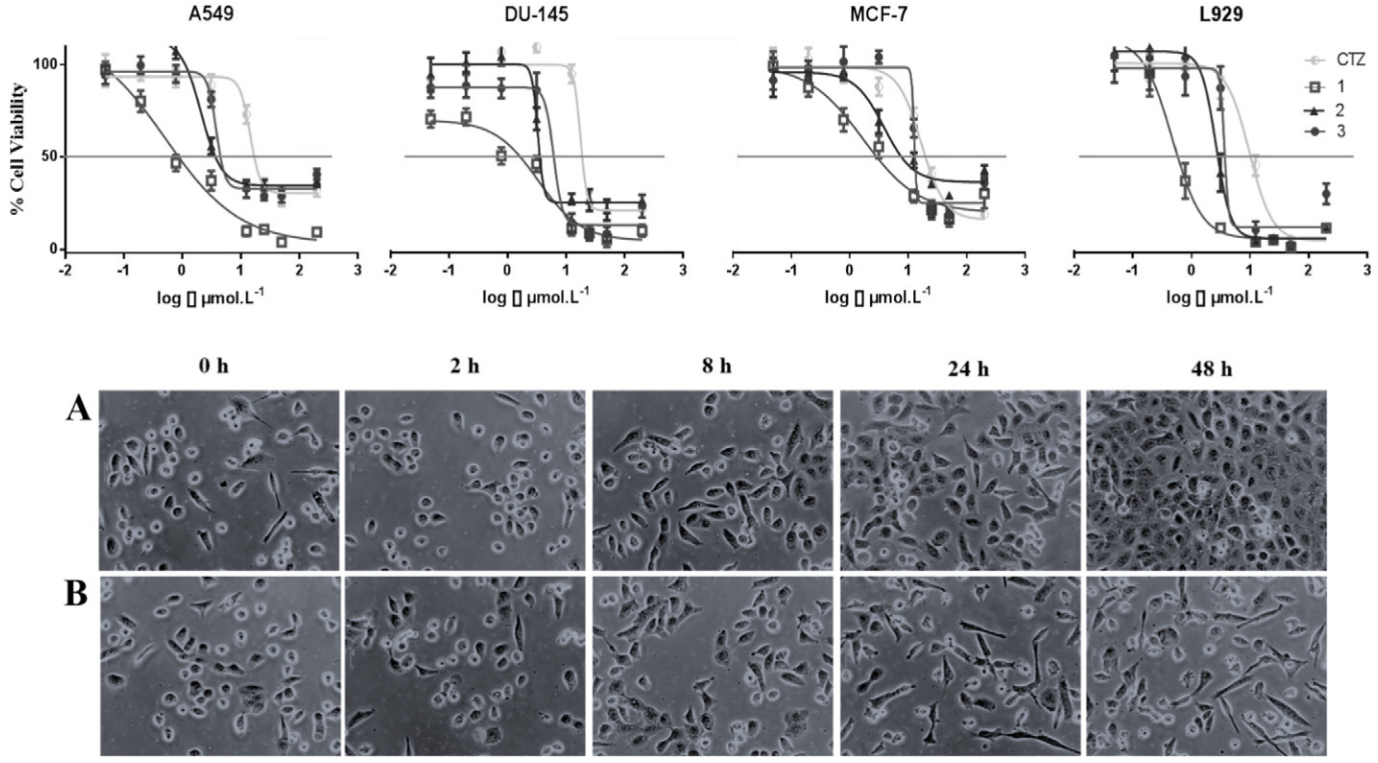

Fig. 7. Upper: MTT colorimetric cell viability assay for the tumor cells lines treated with CTZ, and complexes **1**, **2** and **3** for 48 h. Lower: Morphological study under an inverted microscope (10×) of DU-145 control (A) cells and cells treated (B) with the IC_{50} concentrations of complex **2**. In all panels, the images are representative of many pictures taken in n = 3 experiments.

complex **2** and guanosine or guanosine monophosphate was studied to check the possible lability of the chlorido ligand present in the complex. In Fig. S8 (supplementary information), the ^{1}H and $^{31}P\{^{1}H\}$ NMR spectrum of complex **2** and the mixture of complex **2**: guanosine are shown. As can be seen, after mixing the reagents, no changes were observed in the $^{31}P\{^{1}H\}$ NMR spectrum for complex **2** at different times, indicating that there was not a strong association with the DNA components.

3.2.2. BSA binding studies

Fluorescence spectroscopy is an effective method to explore the interaction between small molecules and macromolecules. To understand the mechanism of interaction between **1** and **3** and BSA, fluorescence quenching experiments were carried out. The fluorescence of BSA comes from its tryptophan, tyrosine and phenylalanine residues, where the latter two contribute to its fluorescence in only a small part [44]. The fluorescence intensity of a compound can be decreased by a variety of molecular interactions, such as excited-state reactions, molecular rearrangements, energy transfer, ground-state complex formation and collision quenching [45]. Static quenching refers to fluorophore–quencher complex formation. Thus, when the temperature is increased, this process occurs less efficiently since the fluorophore–quencher complex is likely to be less stable under the conditions, leading to a decrease in the fluorescence quenching. Moreover, dynamic quenching refers to a process whereby the fluorophore and the quencher come into contact during the lifetime of the excited-state and higher temperatures increase the fluorescence quenching, and as a result the quenching constant increases [46]. In order to ascertain the fluorescence quenching mechanism, the fluorescence quenching data were measured at different temperatures (295 and 310 K), and the results are shown in Table 2.

These results show that K_{SV} for **1**–**3** are directly related to the increase in temperature, indicating that the probable quenching mechanism reaction is initiated by compound formation rather than by dynamic collision. Moreover, the values of K_q were in the range of $(9.18–27.37) \times 10^{13}$ M^{-1} s^{-1} for all complexes, far higher than 2.0×10^{10} M^{-1} s^{-1}, the maximum possible value for dynamic quenching [47], indicating the existence of a static quenching mechanism. The number of binding sites is approximately equal to 1, indicating that there is only one binding site in the BSA for each complex, similar or equal to those reported before for other metal complexes [48].

The interaction forces between drugs and biomolecules may include electrostatic interactions, multiple hydrogen bonds, van der Waals interactions, hydrophobic and steric contacts within the antibody-binding site, *etc.* [49]. The thermodynamic parameters, enthalpy change (ΔH), entropy change (ΔS) and free energy change (ΔG) are the main means used to confirm the binding modes. From the thermodynamic standpoint, $\Delta H > 0$ and $\Delta S > 0$ imply a hydrophobic interaction; $\Delta H < 0$ and $\Delta S < 0$ reflects van der Waals force or hydrogen bond formation; and $\Delta H < 0$ and $\Delta S > 0$ suggests an electrostatic force.

As observed in Table 2, the positive ΔH and ΔS values reveal the predominance of hydrophobic interactions of the compounds with BSA. Furthermore, the negative ΔG values reveal that the interaction process is spontaneous. The magnitude of the BSA-binding constant of complexes **1**–**3**, compared with other Ru(II) complexes reported recently [13], suggests a moderate interaction with BSA molecule.

Table 4
MIC value of antimycobacterial activity for the Ru(II)–CTZ complexes

	MIC (μg/L)	MIC (μM)	IC_{50} (μM)[a]
CTZ	24.23 ± 0.10	70.25 ± 0.28	9.74 ± 2.05
1	12.43 ± 0.09	10.52 ± 0.07	2.61 ± 0.13
2	12.45 ± 0.10	10.30 ± 0.07	0.48 ± 0.05
3	24.82 ± 0.03	18.53 ± 0.02	5.89 ± 0.80

[a] IC50 L929.

3.3. In vitro biological experiments

3.3.1. Growth inhibition assay and morphological observations

Since the 1990s, M–CTZ complexes have been described, where M = Pt(II), Pd(II), Au(I), Ru(II), Cu(II) among other ions, showing that these complexes present a biological potential, mainly against parasites such as *T. cruzi*, *T. brucei* and *Leishmania* and pathogenic agents of neglected diseases such as Trypanosomiasis, Chagas diseases and Leishmaniasis. Recently, a new family of organometallic complexes with formula [Ru(η^6-*p*-cymene)(X)(CTZ)], where X: Cl_2, bipyridine, ethylenediamine or acetylacetonate, have shown high *in vitro* activity against *Leishmania major* and *T. cruzi* and low toxicity toward normal mammalian cells. Therefore, few reports of metal complexes with CTZ have been evaluated against tumor cells. However, free clotrimazole showed a significant decrease in the MCF-7 cell viability, altering its morphological and inhibiting the glycolysis. A comparison with previously reported CTZ metal complexes is significant: in 2006, Pd–$(CTZ)_2$ complex showed very poor cytotoxicity against four human tumor cell lines: MDA-MB-231, PANC-1, SKBR-3 and HT-29, values in the 89–159 μM range [50]. By exchanging the metal center from Pd to Pt, two Pt-$(CTZ)_2$ complexes were reported and both showed inhibitory effects on five cells lines: HT-29, LoVo, MCF-7, SKBR-3 and PC-3 with IC_{50} values in the 5–25 μM range [9]. Current reports (the first in 2012) showed a synergistic effect in the binding of the CTZ to metal ions

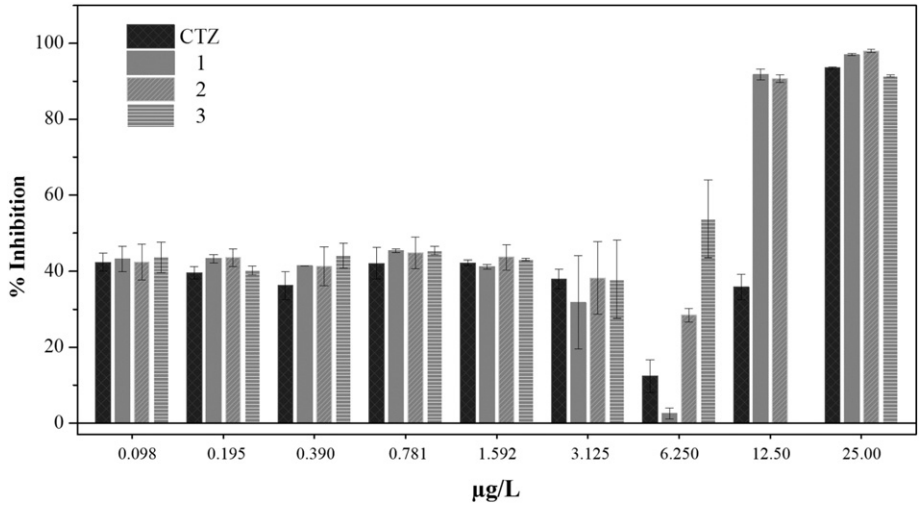

Fig. 8. Perceptual inhibition of *M. tuberculosis* H37Rv with different concentration of CTZ and Ru(II)–CTZ complexes.

such as Cu(II), Co(II), Ni(II), and Zn(II), toward three human carcinoma cells: Hela, PC-3 and HCT-15, with IC_{50} values in the 3.5–29.8 μM range, suggesting that selected Cu(II)-CTZ complexes induce cell death *via* an apoptotic pathway [8]. Furthermore, more recently, in 2013, a series of six Ru–CTZ compounds were studied, showing their activities against three prostate tumor, cervical cancer and lymphoblastic lymphoma cell lines, with IC_{50} values in the 2–546 μM range [7].

Thus, having this in mind, complexes **1**–**3** were evaluated against the A549 (human lung carcinoma), DU-145 (human prostate carcinoma), MCF-7 (human breast carcinoma) and L929 (normal) cell line. The IC_{50} values were calculated from the dose-survival curves obtained after 48 h of Ru(II)–CTZ complexes treatment with an MTT assay (Table 3). The results obtained using this assay show that all three Ru(II)–CTZ complexes presented growth inhibitory effects on three tumor cells lines at doses appreciably lower in comparison with free CTZ, under the same conditions, highlighting the importance of the Ru(II)/bipyridine/phosphine moiety to the antitumor biological activity. For the sake of comparison, the cytotoxicity of cisplatin was evaluated under the same experimental conditions and the complexes were more active against human A549 and complexes **1**–**2** were more active against MCF-7 cell lines than cisplatin. The most remarkable effect was observed in the multidrug-resistant lung cancer cell A549, in which the complexes exert the strongest activity, with IC_{50} values between 0.47 and 4.79 μM. In this cell line, the free ligand shows a much weaker cytotoxicity, yielding an IC_{50} value of 14.47 μM. Under an inverted microscope, cell shape and changes in it can be observed clearly. As shown in Fig. 7, the DU-145 prostate tumor cells show epithelial cell morphology, while in the control group there were very few round cells. Cells treated with complex **2** showed obvious morphological changes after the first 24 h; cells treated for 48 h showed, in addition to morphological changes, a loss of adhesion, a epithelial form and confluence, indicating the possibility of apoptosis.

The values of log D (Table 3) are between the interval 0.48–0.84, so that the biphosphine moiety does not modify significantly lipophilicity for complexes **1**–**3** and no quantitative correlation between lipophilicity and biological activity was observed.

Anti-*M. tuberculosis* activity. The literature describes several cases in which a connection can be made between the structure and activity of coordination compounds, where structural properties can directly interfere with the mechanisms of action of the compounds with anti-*M. tuberculosis* activity. Our research group reported Ru(II) complexes containing byphosphines and bipyridines as binders that were extremely promising, showing minimum inhibitory concentration values similar or better than the current drugs used to treat this disease. Generally, Ru(II) compounds containing bidentate as binders (N–O, N–S or O–O) and two diphosphines or diphosphines/bipyridine ligands show MIC values better than the precursor compound containing chlorido atoms in place of the bidentate ligands. For these reasons, the *in vitro* anti-MTB activities of the free ligand and the Ru(II)–CTZ complexes were tested against MTB H37Rv ATCC 27294 (see Fig. 8). The MIC values are reported in Table 4. The activity found for the complexes is comparable or better than those of some commonly used anti-*M. tuberculosis* agents, such as cycloserine (MIC = 12.50–50 μM), gentamicin (MIC = 4.20–8.40 μM), tobramycin (MIC = 8.56–17.10 μM) and clarithromycin (MIC = 10.70–21.40 μM) [51]. Antimicrobial activity assays of the new complexes provided evidence that complexes **1**, **2** and **3** are potential agents against mycobacterial infections, specifically against *M. tuberculosis* H37Rv.

4. Conclusions

Three complexes combining clotrimazole with different Ru(II)–diphosphine/bipyridine complexes, with general formula $[RuCl(CTZ)(bipy)(P\text{-}P)]PF_6$, were synthesized and characterized by a variety of techniques in a solid state and in solution. The complexes binding to BSA with moderate affinity through a static quenching mechanism and the thermodynamic parameters reveal the predominance of hydrophobic interactions with the protein. The activity of the new compounds was evaluated against three human tumor cell lines and very promising results were obtained, yet all of them had poor selectivity indices (~1) *versus* healthy cells, worse that even cisplatin. Indeed the IC_{50} values of Ru(II)–CTZ complexes on A549 (lung) and MCF-7 (breast) tumor cells lines were lower than those obtained for the free clotrimazole and for the cisplatin (reference drug). The MIC values of anti-*M. tuberculosis* activity obtained for the complexes showed an activity comparable or better than that shown for various second-line drugs used to treat illnesses. They also provided us with evidence that they are potential agents against mycobacterial infections, encouraging the continuation of studies of these types of compounds.

Acknowledgments

We would like to thank CNPq (141738/2013-8 and 141739/2013-4), CAPES, and FAPESP (13/03513-9) for the financial support. We also thank Prof. Dr. Otaciro Nascimento for the CD spectra at IFSC-USP and Dra. Soraya Ochs for the ESI-MS spectra at INMETRO.

Appendix A. Supplementary data

Supplementary data to this article can be found online at http://dx.doi.org/10.1016/j.jinorgbio.2016.06.023.

References

[1] K.H. Büchel, W. Draber, E. Regel, M. Plempel, Arzneimittelforschung 22 (1972) 1260–1272.
[2] (a) J.W. Stocker, L. De Franceschi, G.A. McNaughton-Smith, R. Corrocher, Y. Beuzard, C. Brugnara, Blood 101 (2003) 2412–2418;
(b) N.T. Huy, R. Takano, S. Hara, K. Kamei, Biol. Pharm. Bull 27 (2004) 361–365;
(c) F.S. Buckner, J.A. Urbina, Int. J. Parasitol. Drugs Drug Resist. 2 (2012) 236–242;
(d) H.L. Greenberg, T.A. Shwayder, N. Bieszk, D.P. Fivenson, Pediatr. Dermatol. 19 (2002) 78–81.
[3] R. Palchaudhuri, V. Nesterenko, P.J. Hergenrother, J. Am. Chem. Soc. 130 (2008) 10274–10281.
[4] R.A. Sánchez-Delgado, K. Lazardi, L. Rinch, J.A. Urbina, J. Med. Chem. 36 (1993) (2041-2043 2041).
[5] M. Navarro, E.J. Cisneros-Fajardo, T. Lehmann, R.A. Sánchez-Delgado, R. Atencio, P. Silva, R. Lira, J.A. Urbina, Inorg. Chem. 40 (2001) 6879–6884.
[6] R.A. Sánchez-Delgado, M. Navarro, K. Lazardi, R. Atencio, M. Capparelli, F. Vargas, J.A. Urbina, A. Bouillez, A.F. Noels, D. Masi, Inorg. Chim. Acta 275–276 (1998) 528–540.
[7] A. Martínez, T. Carreon, E. Iniguez, A. Anzellotti, A. Sánchez, M. Tyan, A. Sattler, L. Herrera, R.A. Maldonado, R.A. Sánchez-Delgado, J. Med. Chem. 55 (2012) 3867–3877.
[8] S. Betanzos-Lara, C. Gómez-Ruiz, L.R. Barrón-Sosa, I. Gracia-Mora, M. Flores-Álamo, Noráh öBarba-Behrens, J. Inorg. Biochem. 114 (2012) 82–93.
[9] M. Navarro, A.R. Higuera-Padilla, M. Arsenak, P. Taylor, Trans. Met. Chem. 34 (2009) 869–875.
[10] P.S. Kuhn, V. Pichler, A. Roller, M. Hejl, M.A. Jakupec, W. Kandioller, B.K. Keppler, Dalton Trans. 44 (2015) 659–668.
[11] Z. Adhireksan, G.E. Davey1, P. Campomanes, M. Groessl, C.M. Clavel, H. Yu, A.A. Nazarov, C.H. Fang Y ., W.H. Ang, P. Drge, U. Rothlisberger, P.J. Dyson, C.A. Davey, Nat. Commn. 5:3462 (2014) 1–13.
[12] F.C. Pereira, B.A.V. Lima, A.P. de Lima, W.C. Pires, T. Monteiro, L.F. Magalhães, W. Costa, A.E. Graminha, A.A. Batista, J. Ellena, E. de P. Siveira-Lacerda, J. Inorg. Biochem. 149 (2015) 91–101.
[13] R.S. Correa, K.M. de Oliveira, F.G. Delolo, A. Alvarez, R. Mocelo, A.M. Plutin, M.R. Cominetti, E.E. Castellano, A.A. Batista, J. Inorg. Biochem. 150 (2015) 63–71.
[14] F.B. do Nascimento, G.V. Poelhsitz, F.R. Pavan, D.N. Sato, C.Q.F. Leite, H.S. Selistre-de Araújo, J. Ellena, E.E. Castellano, V.M. Deflon, A.A. Batista, J. Inorg. Biochem. 102 (2008) 1783–1789.
[15] F.R. Pavan, G. Von Poelhsitz, F.B. do Nascimento, S.R.A. Leite, A.A. Batista, V.M. Deflon, D.N. Sato, S.G. Franzblau, C.Q.F. Leite, Eur. J. Med. Chem. 45 (2010) 598–601.
[16] F.R. Pavan, G.V. Poelhsitz, M.I.F. Barbosa, S.R.A.A. Leite, A.A. Batista, J. Ellena, L.S. Sato, S.G. Franzblau, V. Moreno, D. Gambino, C.Q.F. Leite, Eur. J. Med. Chem. 46 (2011) 5099–5107.
[17] E.R. dos Santos, M.A. Mondelli, L.V. Pozzi, R.S. Corrêa, H.S. Salistre-de-Araújo, F.R. Pavan, C.Q.F. Leite, J. Ellena, V.R.S. Malta, S.P. Machado, A.A. Batista, Polyhedron 51 (2013) 292–297.
[18] M.I.F. Barbosa, R.S. Corrêa, L.V. Pozzi, É. de O. Lopes, F.R. Pavan, C.Q.F. Leite, J. Ellena, S. de P. Machado, G. Von Poelhsitz, A.A. Batista, Polyhedron 85 (2015) 376–382.
[19] Global Tuberculosis Report 2015, WHO. (http: www.who.int/tb/data)
[20] P. Bergamini, V. Bertolasi, L. Marvelli, A. Canella, R. Gavioli, N. Mantovani, S. Manas, A. Romerosa, Inorg. Chem. 46 (2007) 4267–4276.

[21] A.A. Batista, M.O. Santiago, C.L. Donicci, I.S. Moreira, P.C. Healy, S.J. Berners-Price, S.L. Queiroz, Polyhedron 20 (2001) 2123–2128.
[22] J. Marmur, J. Mol. Biol. 3 (1961) 11–17.
[23] J.M. Veal, R.L. Rill, Biochem. 30 (1991) 1132–1140.
[24] Serum Albumin, in: T. Peters, F.W. Putman (Eds.), The Plasma Proteins, Academic Press 1975, pp. 133–181.
[25] E. Gratton, N. Silva, G. Mei, N. Rosato, I. Savini, A. Finazzi-Agro, Int. J. Quantum Chem. 42 (1992) 1479–1489.
[26] E. Baka, J.E.A. Comer, K. Takács-Novák, J. Pharm. Biomed. Anal. 46 (2008) 335–341.
[27] J.C. Palomino, A. Martin, M. Camacho, H. Guerra, J. Swings, F. Portaels, Antimicrob. Agents Chemother. 46 (2002) 2720–2722.
[28] W. Geary, J. Coord, Chem. Rev. 7 (1981) 81–122.
[29] S.X. Xiao, W.C. Trogler, D.E. Ellis, Z. Berkovitch-Yellin, J. Am. Chem. Soc. 105 (1983) 7033–7037.
[30] X.J. Yang, C. Janiak, J. Heinze, F. Drepper, P. Mayer, H. Piotrowski, P. Klüfers, Inorg. Chim. Acta 318 (2001) 103–116.
[31] M.Y. Choi, M.C. Chan, S. Zhang, K.K. Cheung, C.M. Che, K.Y. Wong, Organometallics 18 (1999) 2074–2080.
[32] F. Felix, J. Ferguson, H.U. Giidel, A. Ludi, J. Am. Chem. Soc. 102 (1980) 4096–4102.
[33] A.A. Batista, M.O. Santiago, C.L. Donnici, I.S. Moreira, P.C. Healy, S.J. Berners-Price, S.L. Queiroz, Polyhedron 20 (2001) 2123–2128.
[34] S.L. Queiroz, A.A. Batista, G. Oliva, M. Gambardella, R.H.A. Santos, K.S. MacFarlane, S.J. Rettig, B. James, Inorg. Chim. Acta 267 (1998) 209–221.
[35] A.M. Pyle, J.P. Rehmann, R. Meshoyrer, C.V. Kumar, N.J. Turro, J.K. Barton, J. Am. Chem. Soc. 111 (1989) 3051–3058.
[36] H. Zipper, H. Brunner, J. Bernhagen, F. Vitzthum, Nucleic Acids Res. 32 (2004), e103.
[37] W. Villarreal, L. Colina-Vegas, C.R. de Oliveira, J.C. Tenorio, J. Ellena, F.C. Gozzo, M.R. Cominetti, A.G. Ferreira, M.A.B. Ferreira, M. Navarro, A.A. Batista, Inorg. Chem. 54 (2015) 11709–11720.
[38] A. Sellamuthu, R. Ravishankaran, A.A. Karande, M. Kandaswamy, Dalton Trans. 41 (2012) 12970–12983.
[39] B.C. Baguley, M.L. Bret, Biochem. 23 (1984) 937–943.
[40] K.G. Strothkamp, R.E. Strothkamp, J. Chem. Educ. 71 (1994) 77–79.
[41] P. Živec, F. Perdih, I. Turel, G. Giester, G. Psomas, J. Inorg. Biochem. 117 (2012) 35–47.
[42] V. Rajendiran, M. Murali, E. Suresh, M. Palaniandavar, V.S. Periasamyc, M.A. Akbarshac, Dalton Trans. (2008) 2157–2170.
[43] A. Ghosh, A. Mandoli, D.K. Kumar, N.S. Yadav, T. Ghosh, B. Jha, J.A. Thomas, Dalton Trans. (2009) 9312–9321.
[44] D.C. Carter, J.X. Ho, Adv. Prot. Chem. 45 (1994) 153–203.
[45] J.R. Lakowicz, Biochem. 12 (1973) 4161–4170.
[46] L. Shang, Y.Z. Wang, J.G. Jiang, S.J. Dong, Langmuir 23 (2007) 2714–2719.
[47] X. Zhao, R. Liu, Z. Chi, Y. Teng, P. Qin, J. Phys. Chem. B 114 (2010) 5625–5631.
[48] V. Sankareswari, D. Vinod, A. Mahalakshmi, M. Alamelu, G. Kumaresan, R. Ramaraj, S. Rajagopal, Dalton Trans. 43 (2014) 3260–3272.
[49] P.D. Ross, S. Subramanian, Biochem. 103 (1981) 3096–3104.
[50] M. Navarro, N.P. Pena, I. Colmenares, T. González, M. Arsenak, P. Taylor, J. Inorg. Biochem. 100 (2006) 152–157.
[51] S.G. Franzblau, R.S. Witzig, J.C. McLaughlin, P. Torres, G. Madico, A. Hernandez, M.T. Degnan, M.B. Cook, V.K. Quenzer, R.M. Ferguson, R.H. Gilman, J. Clin. Microbiol. 36 (1998) 362.